Remaining Useful Life Prediction and State of Health Diagnosis for Lithium-Ion Batteries Using Particle Filter and Support Vector Regression

Jingwen Wei, *Student Member, IEEE*, Guangzhong Dong, *Member, IEEE*, and Zonghai Chen, *Member, IEEE*

***Abstract*—Accurate remaining useful life (RUL) prediction and state-of-health (SOH) diagnosis are of extreme importance for safety, durability, and cost of energy storage systems based on lithium-ion batteries. It is also a crucial challenge for energy storage systems to predict RUL and diagnose SOH of batteries due to the complicated aging mechanism. In this paper, a novel method for battery RUL prediction and SOH estimation is proposed. First, a novel support vector regression-based battery SOH state-space model is established to simulate the battery aging mechanism, which takes the capacity as the state variable and takes the representative features during a constant-current and constant-voltage protocol as the input variables. The estimated impedance variables are taken as the output due to the correlation between battery capacity and the sum of charge transfer resistance and electrolyte resistance. Second, in order to suppress the measurement noises of current and voltage, a particle filter is employed to estimate the impedance degradation parameters. Furthermore, experiments are conducted to validate the proposed method. The results show that the proposed SOH estimation method can provide an accurate and robustness result. The proposed RUL prediction framework can also ensure an accurate RUL prediction result.**

***Index Terms*—Energy storage, health monitoring, state estimation, support vector regression (SVR).**

I. Introduction

DUE to the growing concern over fuel consumption and carbon emissions, low-emission and energy-saving electric vehicles (EVs) and microgrids have become the developing tendency of energy transformation and supply. Lithium-ion batteries (LIBs) have become widely used power sources in EVs and energy storage systems in microgrids due to their high power density, high energy density, and long lifetime [1], [2]. One of the most important issues in the utilization of LIB is to determine its remaining useful life (RUL) and diagnose its state-of-health (SOH), due to the electrical properties, safety and stability alterations of LIB would change with battery RUL and SOH [3], [4]. The RUL can be regarded as the length of time from present time to the end of total useful life [5], while SOH represents the battery aging level reflected on battery parameters such as total useful capacity reduction and resistance increase [6]. The accurate RUL prediction and SOH diagnosis for LIB-based energy storage systems can provide the battery performance variance during its whole service life and can also improve battery management techniques to extend battery life and understand more accurate battery operation parameters.

A battery's use generates irreversible physical and chemical changes, and thus the electrical properties tend to deteriorate gradually over its lifetime, such as capacity decrease and resistance increase [7]. The SOH is often defined as a percentage that reflects internal resistance increase and capacity decrease. For instance, SOH is defined as 100% for a fresh cell, while SOH is 0% for the cell that reaches limitations of the end-of-life (EoL). The most common definition of limitation is when the capacity reaches its 70–80% of the nominal capacity. Another limitation based on internal resistance is when it increases to 160% of its initial value for the same SOC and operating temperature condition [6]. As one of the most important aspects of battery health management, RUL is defined as the length of time from present time to the EoL, the issue of predicting battery's RUL could thus be transformed to approximate the probability distribution function (PDF) of the time when its capacity or internal resistance crosses predefined failure limitations [5].

There are various research works on SOH estimation and RUL prediction. The SOH of a battery can be estimated by applying processes and algorithms to its measurable parameters, like terminal voltage, current, and temperature. These algorithms or processes can transform these parameters into SOH and RUL. According to Hu *et al.* [8], [9], these processes and algorithms for SOH and/or RUL can be principally classified into four categories: 1) direct measurement; 2) battery model-based parameters identification closed-loop estimation; 3) durability model based open-loop estimation; and 4) data-driven method.

1) *Direct measurement:* A direct measurement for determining battery capacity is to completely discharge a cell after a full charging process, which follows a constant-current and

Manuscript received March 27, 2017; revised June 6, 2017, July 25, 2017, and October 25, 2017; accepted November 19, 2017. Date of publication December 11, 2017; date of current version March 6, 2018. This work was supported by the National Natural Science Fund of China under Grant 61375079. *(Corresponding author: Zonghai Chen.)*

The authors are with the Department of Automation, University of Science and Technology of China, Hefei 230026, China (e-mail: wei0519@mail.ustc.edu.cn; dgz0725@mail.ustc.edu.cn; chenzh@ustc.edu.cn).

Color versions of one or more of the figures in this paper are available online at http://ieeexplore.ieee.org.

Digital Object Identifier 10.1109/TIE.2017.2782224

constant-voltage (CC and CV) protocol for LIB. The battery static capacity is then calibrated. Coulomb counting is one of the most commonly used methods. After the battery is fully charged, the Coulomb counting method is employed to calculate discharged battery capacity. SOH can then be determined by dividing the fully discharged capacity with the value of rated capacity. This method is simple and easy to implement. However, Coulomb counting is an open-loop method that requires battery fully charged and fully discharged during one cycle, which is inconvenient, practically. As to internal resistance, the hybrid pulse power characterization method is often used to measure battery resistance at different state of charges (SOCs) and temperature conditions [10]. These methods are the most accurate measurement techniques but have only limited application, e.g., a laboratory environment. However, they are impractical in realistic operations, as the energy is wasted by the test and they are time-consuming.

2) *Battery model-based parameters identification closed-loop estimation:* In order to overcome the drawbacks of the *direct measurement* methods, the open-loop-based capacity and resistance estimation method should be converted to an adaptive one. Thus, the *battery model-based parameters identification closed-loop estimation methods* are introduced. These methods treat battery SOH estimation issue as a parameter estimation problem based on a battery model describing dynamic characteristic. Lots of SOH observers have been proposed based on electrical circuit or electrochemical models. For instance, dual extended Kalman filtering (EKF) in [11]–[13], particle filtering (PF) in [14], dual slide mode observer in [15], and Lyapunov-based adaptive observer in [6] and [7]. These methods are online and closed-loop. However, due to the coupling relationship between SOH and SOC, the erroneous SOC estimation will lead to inaccurate SOH estimation. The inaccurate SOH will increase the SOC error in turn. Besides, the selected battery models play an important role in effectiveness and adaptability of the estimation algorithms.

3) *Durability model based open-loop estimation:* Despite the battery model based parameters identification methods, which employ the discharging/charging current and voltage to extract the degradation parameters, like capacity and resistance, some works developed durability models based on battery aging test experiments. For instance, Wang *et al.* [16] established a cycle-life model to portray the capacity fade of graphite/LiFePO4 cells as a function of temperature, depth of discharge, and discharge rate (C-rate). Cell life data for establishing the model were collected using a large cycle-test matrix. Data fitting approaches were employed to create the cycle-life model. Saxena *et al.* [17] quantified the effect of partial charge–discharge cycling on graphite/LiCoO2 battery capacity loss by means of cycling tests under different SOC ranges and discharge currents. These methods predict directly the capacity fade and the internal resistance changes based on a battery durability model. To obtain a battery durability model, the batteries are cycled or stored at specific conditions. Then, an empirical formula is established to find the relationship between capacity loss or internal resistance and the cycle numbers/time, while temperature is also taken into consideration. Matsushima [18] found that capacity loss exhibited a square root relationship with time. These open-loop models are simple and easy to implement. However, these offline models provide no insight into detailed electrochemical processes incurring battery aging. These semi empirical models also highly depend on the quality of testing data.

4) *Data-driven methods:* The data-driven methods are flexible and model-free. During battery operation cycles, some achievable variables or representative features can be used to predict battery SOH. For instance, incremental capacity analysis [19] and differential voltage analysis [20] methods are the basic methodologies to find mapping from battery features to SOH based on signal processing techniques. Wang *et al.* [20] showed the linear regression of the location interval between two inflection points versus the battery capacity. These methods are simple. However, the numerical SOH estimations are not directly inferred. The further manipulation must be designed based on the signal processing results. These techniques include a center least squares method [20], etc. Besides, these techniques are not suitable for onboard applications. To overcome these drawbacks, some mapping techniques were introduced based on black-box models and machine learning tools. These models or tools took the achievable variables or representative features extracted as the input, and took SOH as the output. For instance, artificial neural networks (ANN) [4], support vector machine (SVM) [21], fuzzy logic [22], sparse Bayesian prediction [8], PF [23], and multiorder PF [24]. These techniques are featured with good nonlinear regression performance. However, most of these methods focus on data regression. For example, both Dong *et al.* [23] and Jiang *et al.* [24] employed PF to smooth battery data, while SVM was employed to rebuild posterior distributions of a particle, and multiorder mechanism was employed to include past data samples for future estimation. They pay little attention to the dynamic characteristics of the battery aging mechanism. Namely, the aging mechanism between two adjacent cycles is not well explained. One of the most effective representations for these dynamics is a state-space model.

In order to establish the state transition model to describe system dynamic characteristics, the data-driven algorithms including ANN, SVM, and Gaussian process regression (GPR), etc., have been utilized. For instance, Charkhgard and Farrokhi [25] presented a battery state-space model based on a radial basis function (RBF) NN, then the EKF was employed to estimate battery SOC based on the proposed battery model. Asefa *et al.* [26] used the SVM to reconstruct a nonlinear state-space model, and Qin *et al.* [27] applied particle swam optimization for obtaining the support vector regression (SVR) kernel parameters. Li and Xu [28] presented an integrated approach based on a mixture of Gaussian process model and PF for LIB SOH estimation under uncertain conditions, where the distribution of the degradation state-space model was learnt from the inputs based on the available capacity monitoring data using GPR, while the PF was implemented to predict the battery SOH by exploiting the distribution information of the degradation model parameters. Saha *et al.* [29] used the relevance vector machine, which was a Bayesian form representing a generalized linear model of identical functional form of the SVM, for diagnosis as well as for model development. The PF framework then used

the established model and statistical estimates of the noise in the system and anticipated operational conditions to provide estimations of SOC, SOH, and RUL. These techniques first employ a data-driven method to establish a battery degradation state-space model. Then, the adaptive filtering like Kalman filter and particle filter is employed for SOH and RUL estimation purposes.

The main contribution of this paper is to build a previously mentioned state-space model to represent battery aging dynamics using the SVR method. The state-space model is built to describe the degradation parameters based on the analysis of battery aging behaviors. Based on this SVR-based state-space model, an SOH prognosis and RUL prediction framework is further proposed using PF. In order to establish the degradation model, the most important issue is to define a set of input, output, and state variables related to first-order differential equation. Therefore, key achievable variables or representative features extracted are first analyzed. The state variables, input, and output of the state-space model are then defined, while the mathematical formula of state equation and output equation is established. Based on the proposed model, the issue of predicting batteries' SOH could, thus, be transformed to a state estimation problem. In this sense, one of the advantages of this framework is that it can regress the aging mechanism between two adjacent cycles. Besides, the algorithm can suffer from erroneous initial state value and parameter perturbation.

Because of the complex electrochemical reaction process, it is impossible to find an analytic expression for this state-space model. Therefore, an SVR-based battery capacity degradation model is established to simulate the battery aging mechanism, which takes the capacity as the state variable, and takes the representative features during a CV protocol as the input variables. The estimated impedance variables are taken as the output due to the correlation between battery capacity and the sum of charge transfer resistance and electrolyte resistance. Finally, a PF is employed to estimate the degradation parameters in order to suppress modeling inconsistencies, the system noise, and degraded sensor fidelity.

The rest of this paper is outlined as follows. Section II presents the experimental data analysis. The SVR-based battery capacity degradation model, state-space model for degradation parameters, and PF are introduced in Section III. Section IV discusses the verification and experimental results. Conclusions and remarks are summarized in Section V.

II. Test Data Analysis

Experimental data from second-generation, Gen 2, 18650-size LIBs produced by Idaho National Laboratory [30] are used in this paper. A set of four LIBs was run through three different operational profiles (charge, discharge, and impedance) at room temperature. As shown in Fig. 1, charging was carried out in a CC and CV mode, where the constant current was 1.5 A until the battery voltage reached 4.2 V, and then constant voltage was continued until charge current dropped to 20 mA. Discharging was carried out at a 2 A constant current until battery voltage reached to 2.7, 2.5, and 2.2 V for different cells. It should be noted that the charge process for all cells was the same.

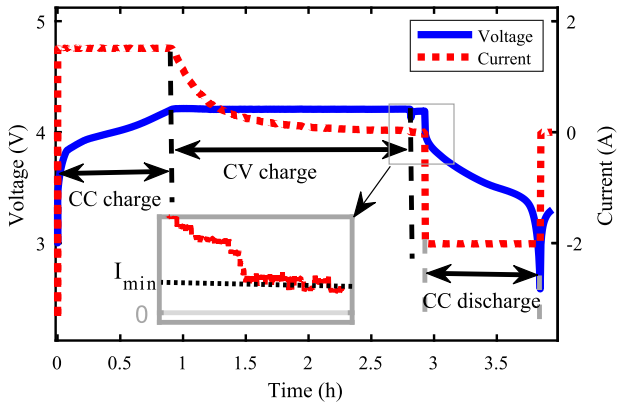

Fig. 1. Battery terminal voltage during one cycle.

TABLE I
Details of Experimental Dataset

Cell num.	Cycle profiles description.		
	Cutoff voltage (V)	Discharge current	Temperature (ºC)
5#	2.7	2 A @CC	24
6#	2.5	2 A @CC	24
7#	2.2	2 A @CC	24
18#	2.5	2 A @CC	24

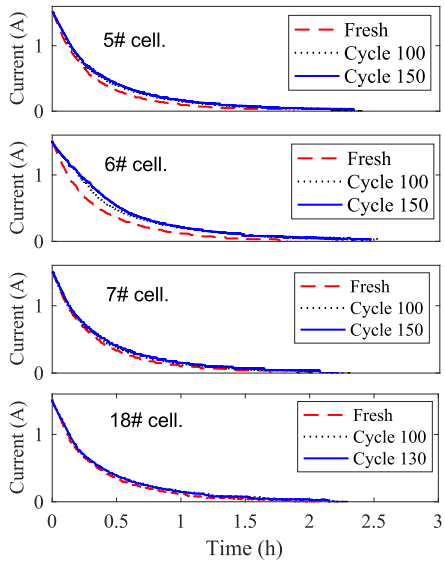

Fig. 2. Charge current during a constant voltage stage of four cells at different aging times.

However, the cutoff voltage was different for every cell. The details are presented in Table I. The battery cycles were repeated to accelerated degradation, while impedance measurements provided insights into how the internal battery parameters changed.

The battery currents during the CV stage change at different aging times for the test cells. The charging currents vary exponentially with cycle number. As shown in Fig. 2, the charging currents of the four cells show different time constants and charging capacities at different aging times. Herein, the exponential function as in the following equation is used to simulate

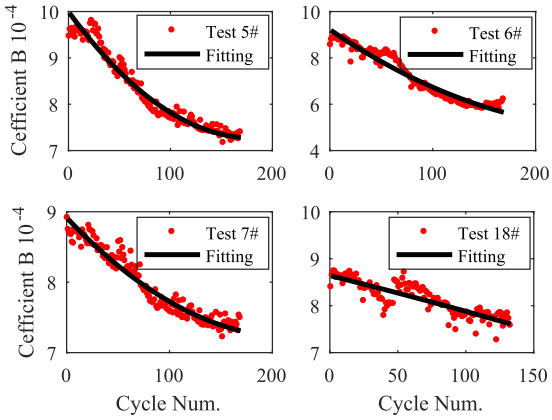

Fig. 3. Coefficient B versus cycle num. for four cells during the CV stage.

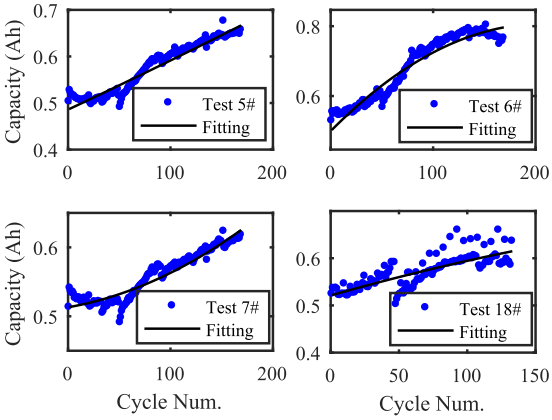

Fig. 4. Charged capacity versus cycle num. for four cells during the CV stage.

the battery current behavior at the CV stage ($t = 0$ corresponding to the beginning of the CV charging) [31]:

$$I(t) = A\exp(-Bt) + C \tag{1}$$

where I is the battery current, t is the sampling time ($t = 0$ corresponding to the beginning of the CV mode), and A, B, C are the model parameters.

The identified time constant B of the four cells is plotted in Fig. 3, while the charged capacity during the CV stage of the four cells is plotted in Fig. 4. It is shown in Figs. 3 and 4 that the time constant B changes decrease with the cycle number, while the charged capacity during the CV stage increases with the cycle number. The quadratic functions are employed to simulate the relationship among the time constant B, charged capacity, and the cycle number as follows:

$$B(k) = a_B k^2 + b_B k + c_B. \tag{2}$$

$$Q_{\mathrm{CV}}(k) = a_Q k^2 + b_Q k + c_Q \tag{3}$$

where B is the time constant, Q_{CV} is the charged capacity during the CV stage, a_B, b_B, c_B, a_Q, b_Q, and c_Q are the model parameters, and k is the cycle number. The identified parameters are listed in Table II.

TABLE II
IDENTIFIED PARAMETERS FOR EXPERIMENTAL DATA

Cell num.	Cell 5	Cell 6	Cell 7	Cell 18
$a_B\,(\cdot 10^{-9})$	8.81	6.16	3.82	−38.8
$b_B\,(\cdot 10^{-6})$	−3.08	−3.15	−1.60	−72.2
$c_B\,(\cdot 10^{-4})$	9.98	9.23	8.92	8.64
$a_Q\,(\cdot 10^{-8})$	−7.59	−783	225	−88.8
$b_Q\,(\cdot 10^{-4})$	10.9	30.8	2.97	8.23
$c_Q\,(\cdot 10^{-1})$	4.86	4.99	5.13	5.21

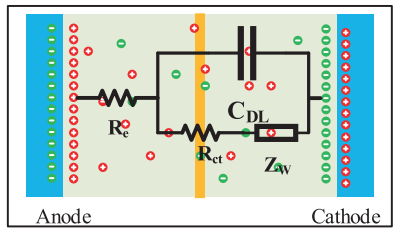

Fig. 5. Equivalent circuit for a single cell of battery impedance.

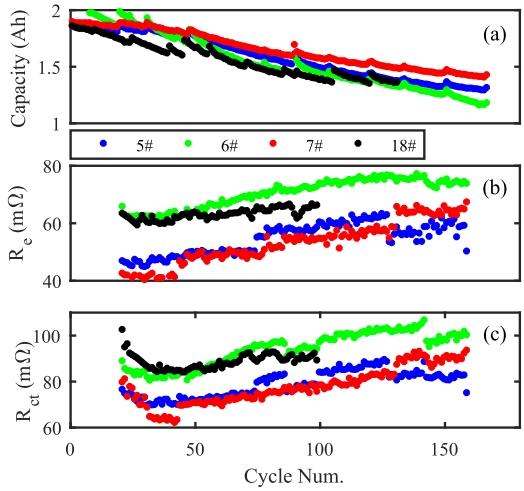

Fig. 6. (a) Capacity degradation, (b) R_e, and (c) R_{ct} degradation.

The impedance degrades as a function of cycle number when the battery ages. To describe the internal parameters, the lumped parameter battery model shown in Fig. 5 [30] is employed. The parameters of this battery model can be estimated from impedance data. The parameters of major interest are the double-layer capacitance C_{DL}, the charge transfer resistance R_{ct}, the Warburg impedance Z_W, and the electrolyte resistance R_e. The relationship among capacity degradation, R_e, R_{ct}, and the cycle number is plotted in Fig. 6(a)–(c). It can be seen from Fig. 7 that there was a high degree of correlation among the impedance $R_e + R_{\mathrm{ct}}$, battery capacity, and the cycle number. The capacity and impedance $R_e + R_{\mathrm{ct}}$ show a linear correlation. Besides, according to [30], the time dependent of impedance

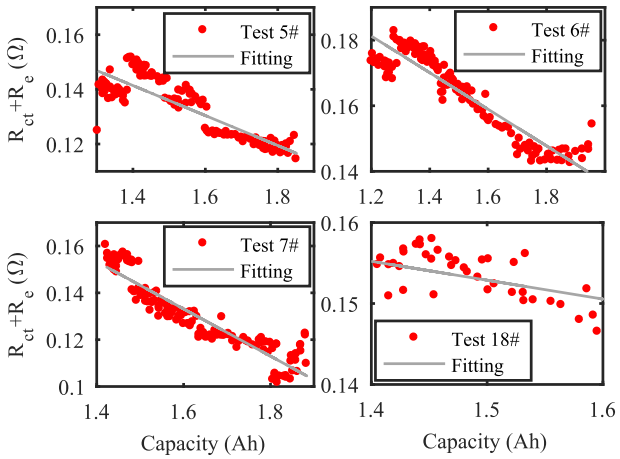

Fig. 7. Impedance $R_e + R_{\text{ct}}$ versus capacity of the four cells.

can be modeled by an exponential equation, as follows:

$$R_t = R_0 \exp(\lambda_R t) \tag{4}$$

where R_t represents the battery impedance (R_e, R_{ct}) at time t. R_0 is a fitting constant. λ_R is a battery aging parameter. Equation (4) can be discretized as the following equation, in order to build a state-space model to estimate battery degradation parameter:

$$\begin{cases} \lambda_R(k) = \lambda_R(k-1) + w_1(k) \\ x_R(k) = x_R(k-1)\exp(\lambda_R(k-1)\cdot\Delta k) + w_2(k) \\ R(k) = x_R(k) + v(k) \end{cases} \tag{5}$$

where k is the corresponding cycle number. $\lambda_R(k)$ represents the degradation parameter at cycle number k. x_R is the smoothed impedance value. The first and second equation can be regarded as state equation, while the third one is the output equation. $w_1(k), w_2(k)$, and $v(k)$ represent system and output noises with covariance Q_{w1}, Q_{w2}, and Q_v, respectively. Based on (5), the battery impedance degradation parameter can be estimated by using PF.

III. Modeling and Methods

The main objective of this study is to develop a state-space representation for describing the battery aging mechanism and provide a prognostic algorithm for battery SOH estimation and RUL prediction. Herein, the SVR-based capacity degradation model is established, while PF is employed to estimate the degradation parameters according to impedance measurements at every cycle.

A. Capacity Degradation Model

It is necessary for battery SOH estimation or RUL prediction algorithm to get achievable variables or features extracted. However, it is impossible to achieve variables or features extracted from the same or similar driving conditions for different battery cycles during a battery discharging process. On the contrary, CC and CV is a widely used protocol to fully charge cells. Though the charge current is constant during the CC mode and the cutoff voltage of every different cycle number is the same, the start of the CC mode is difficult to know in real applications. During the CV mode, as can be seen from Fig. 1, the beginning, ending, and the charging voltage are all the same under different cycle numbers. Therefore, the variables and features extracted are all achieved during the CV mode in state equations. At the end of the discharging process (SOC $= 0\%$), the impedance variables are estimated from impedance test to update SOH/RUL.

1) SVR-Based Capacity Degradation Model: In order to describe the battery capacity degradation mechanism, the state variable is taken as the battery capacity C_d. As the correlation between coefficient B in (2), charged capacity during the CV mode Q_{CV} in (3), and C_d, B, and Q_{CV} can be taken as the input variables. Thus, the issue to establish the degradation model could be transformed to find the correlation between these two variables and the capacity degradation, as follows:

$$C_d(k+1) = f(C_d(k), B(k), Q_{\text{CV}}(k)) + \omega(k) \tag{6}$$

where $f(C_d(k), B(k), Q_{\text{CV}}(k))$ is a function used to describe the degradation mechanism, and $\omega(k)$ represents the model error. Because of the complex electrochemical reaction process, it is impossible to find an analytic expression for this equation. The SVR algorithm is employed to approximate (6). SVM is first designed to solve the nonlinear two-class classification problem. An SVM for regression can be trained to predict physical parameter. For the given training dataset $T = \{(\boldsymbol{x}_1, \boldsymbol{y}_1), (\boldsymbol{x}_2, \boldsymbol{y}_2), ..., (\boldsymbol{x}_l, \boldsymbol{y}_l)\}, \boldsymbol{x}_i \in X = R^n, \boldsymbol{y}_i \in Y = R, (i = 1, 2, ..., l)$, the SVR can transform the space of the inputs to a higher dimensional feature space through nonlinear transformation defined by the inner product of kernel function. Then, regression issues that cannot be linear regressed in the space of the inputs might be regressed in a higher dimensional feature space, which can be formulated as

$$f(\boldsymbol{x}) = \boldsymbol{w}\phi(\boldsymbol{x}) + \boldsymbol{b} \tag{7}$$

where $f(\boldsymbol{x})$ represents the approximation for capacity degradation. $\boldsymbol{x}, \boldsymbol{w}$, and $\boldsymbol{b}$ are the input data, the weight, and the intercept. $\phi(\boldsymbol{x})$ is the feature space The goal of the SVR is to find a function such that the maximum deviation of $f(\boldsymbol{x})$ from a training data is less than a predefined value ε while maintaining the highest possible flatness. By introducing the slack variable $\{\xi_i\}_{i=1}^l, \{\xi_i^*\}_{i=1}^l$, $\boldsymbol{w}$ and $\boldsymbol{b}$ can be obtained by minimizing the objective function (8) subject to the constraints (9) as follows:

$$\min_{\boldsymbol{w}} R(\xi_i, \xi_i^*, \boldsymbol{w}) = 1/2\|\boldsymbol{w}\| + C\sum_i (\xi_i + \xi_i^*). \tag{8}$$

$$\text{s.t.} \begin{cases} \boldsymbol{y}_i - \boldsymbol{w}\phi(\boldsymbol{x}_i) - \boldsymbol{b} \le \varepsilon + \xi_i. \\ -\boldsymbol{y}_i + \boldsymbol{w}\phi(\boldsymbol{x}_i) + \boldsymbol{b} \le \varepsilon + \xi_i^*. \\ \xi_i \ge 0; \xi_i^* \ge 0. \end{cases} \tag{9}$$

By means of the Lagrange duality, the dual problem of the (6) can be deduced. The issue to find optimal solution w and b can

be transformed to optimal of the Lagrangian

$$\min_{\alpha^{(*)}\in R^{2l}} 1/2\sum_{i,j}(\alpha_i^{(*)}-\alpha_i)(\alpha_j^{(*)}-\alpha_j)[\phi(\boldsymbol{x}_i)\phi(\boldsymbol{x}_j)] + \varepsilon\sum_i(\alpha_i^{(*)}+\alpha_i) - \sum_i \boldsymbol{y}_i(\alpha_i^{(*)}-\alpha_i) \quad (10)$$

subject to

$$\text{s.t.}\begin{cases}\sum_i(\alpha_i^{(*)}-\alpha_i)=0;\\ 0\le\alpha_i^{(*)}\le C, \quad i=1,2,...,l\end{cases} \quad (11)$$

where $\alpha_i^{(*)}=\{\alpha_i,\alpha_i^*\}$ are the Lagrange multipliers. The resultant optimized target function has the following form:

$$f(\boldsymbol{x}) = \boldsymbol{w}\phi(\boldsymbol{x})+\boldsymbol{b} = \sum_i K(\boldsymbol{x}_i,\boldsymbol{x})(\alpha_i^{(*)}-\alpha_i)+\boldsymbol{b} \quad (12)$$

where $K(\boldsymbol{x}_i,\boldsymbol{x})=\phi(\boldsymbol{x}_i)\phi(\boldsymbol{x}_j)$ is the kernel function. The RBF kernel is the most popular choice, which can be represented as

$$K(\boldsymbol{x}_i,\boldsymbol{x})=\exp(-\gamma\|\boldsymbol{x}_i-\boldsymbol{x}\|^2) \quad (13)$$

where γ is the radius of the RBF kernel function.

2) Impedance Aging-Based Battery Degradation Parameter Model: The LIB degradation is dominantly affected by the formation of a solid electrolyte interface consuming free lithium and growing a surface layer. This results in increasing internal resistance and decreasing capacity degradation, as can be seen in Fig. 6. In this study, the capacity degradation is simulated based on the SVR model, where the input of this SVR-based model is the extracted $B(k)$ and $Q_{\text{CV}}(k)$. However, in some cases, the charging scheme does not follow the CC and CV scheme. In these cases, $B(k)$ and $Q_{\text{CV}}(k)$ can be predicted or guessed from (2) and (3). Therefore, the SVR-based capacity degradation model may introduce prediction errors. To overcome these issues, the impedance aging-based degradation parameter model is established to improve the reliability of the SVR-based prediction results. Here, a Gaussian distribution $N(\epsilon(k),\delta_k^2)$ is chosen to improve capacity prediction results, where the mean value $\epsilon(k)$ is the predicted battery capacity according to the SVR-based capacity degradation model (as shown in the following equation), the variance δ_k^2 can be formularized as follows based on the impedance degradation parameter, whose model has been shown in (5):

$$\begin{cases}\epsilon(k+1)=C_d(k+1)=f(C_d(k),B(k),Q_{\text{CV}}(k))+\omega(k);\\ \delta_{k+1}^2=(C_d(k)\exp(-\lambda_R(k))-\epsilon(k+1))^2.\end{cases} \quad (14)$$

As seen from Fig. 7, the internal impedance parameter R_e+R_{ct} shows a high degree of linear correlation with the battery capacity. The impedance degradation parameter λ_R could, thus, reflect a battery capacity degradation rate. Therefore, in order to predict battery capacity at cycle k, first, the SVR-based capacity degradation model in (6) is employed to capture the mean value $\epsilon(k)$. When the charging scheme does not follow the CC and CV scheme, (2) and (3) are used to simulate $B(k)$ and $Q_{\text{CV}}(k)$. Second, the impedance-based degradation parameter λ_R is online estimated using PF. Finally, the predicted capacity is regarded as a Gaussian distribution, where the variance δ_k^2 is expressed as (14).

B. Particle Filtering

PF is a general algorithm based on the recursive Bayesian estimation, which uses the Monte Carlo method to draw particles from a posterior distribution and assigns a weight to each particle. It focuses on a general situation for nonlinear state-space model and non-Gaussian noise assumption, while the KF family, like EKF or unscented KF, is based on a local linearized state-space model and Gaussian noise assumption. For the system, the state-space model for PF is as shown in (5), and the state distribution is represented by a set of samples while using the PF method. The PF algorithm is as reviewed in [1]. According to the procedures of the particle filter, the algorithm can be performed as follows.

1) Initialization: $k=0$, randomly generate N initial particles $[\lambda_R^i(0),x_R^i(0)]^T,(i=1,2,...,N)$ for state variables;
2) For $k=1,2,...$
   a) Particle updating: generate N particles $[\lambda_R^i(k),x_R^i(k)]^T$ according to (5) and the last sampled N particles $[\lambda_R^i(k-1),x_R^i(k-1)]^T$, as follows:

$$\begin{cases}\lambda_R^i(k)=\lambda_R^i(k-1)+w_1(k)\\ x_R^i(k)=x_R^i(k-1)\exp(\lambda_R^i(k-1)\cdot\Delta k)+w_2(k).\end{cases} \quad (15)$$

   b) Importance sampling: the particle weight $\omega^i(k)$ is calculated according to the following equation:

$$\omega^i(k)=1/\sqrt{2\pi Q_v}\exp(-(R(k)-R^i(k))^2/2Q_v) \quad (16)$$

   where $R^i(k)=x_R^i(k)$. $R(k)$ is the measured impedance value.
   c) Normalize the importance weights as

$$\omega^i(k)=\omega^i(k)/\sum_{i=1}^N\omega^i(k). \quad (17)$$

   d) Now a set of *posteriori* particles $C_d^i(k)$ can be generated on the basis of the weights $\omega^i(k)$ by a multinomial resampling method.
   e) The λ_R estimation results are

$$\begin{cases}\widehat{\lambda}_R(k)=\sum_{i=1}^N\omega^i(k)\lambda_R^i(k)\\ \widehat{x}_R(k)=\sum_{i=1}^N\omega^i(k)x_R^i(k).\end{cases} \quad (18)$$

C. Proposed SOH Estimation Method

In order to estimate battery SOH based on the proposed method, an offline SVR model is first trained and some key parameters are also offline fitted, such as B and Q_{CV}. The SOH estimation task can be divided into three steps. First, the PF method must be initialized. Second, the time update process is used to update the particles using the state equation in (15). Besides, the capacity at cycle number k is estimated using the

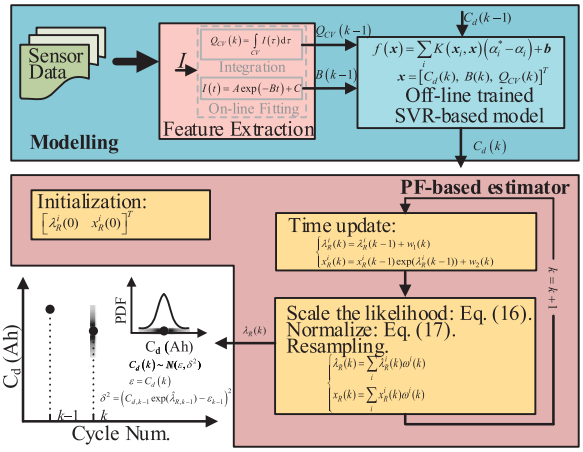

Fig. 8. Flowchart of the SOH estimation algorithm.

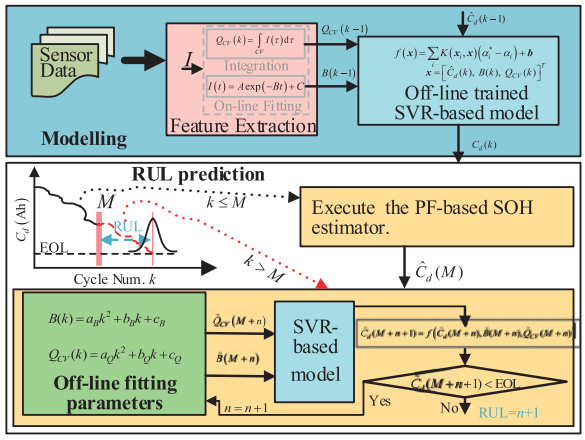

Fig. 9. Flowchart of the RUL prediction method.

SVR-based model, where the input is the capacity at cycle number k, $C_d(k)$, the extracted feature from sensor data during the CV charging mode at cycle number k, $Q_{\mathrm{CV}}(k)$, and $B(k)$. Third, the likelihood of the updated particles is scaled using (16). The particles can be resampled according to the normalized importance weights. After the PF-based estimator, the predicted capacity at cycle number k, $\tilde{C}_d(k)$ is regarded as a Gaussian distribution, whose mean value and variance follow (14). The SOH can be further formulated as the ratio between the estimated capacity $\tilde{C}_d(k)$ and the capacity of a fresh cell $C_d(0)$. The flowchart of the proposed method can be viewed by drawing a block diagram, as shown in Fig. 8.

D. Proposed RUL Prediction Method

In order to predict battery RUL based on the SVR-based model at cycle number M, the following steps must be executed. First, a counter n must be initialized. Second, for $n \geq 1$, the predicted capacity at cycle number $M+n$ can be updated by

$$\begin{cases} \epsilon(t+1) = \tilde{C}_d(t+1) = f(\tilde{C}_d(t), \tilde{B}(t), \tilde{Q}_{\mathrm{CV}}(t))|_{t=M+n-1}; \\ \delta^2_{t+1} = (C_d(M)\exp(-\bar{\lambda}_{R,1:M} \cdot (n+1)) - \epsilon(t))^2|_{t=M+n-1} \end{cases} \tag{19}$$

where $\tilde{C}_d(M+n)$ is predicted capacity at cycle number $M+n$. The inputs of the SVR-based model at cycle number $M+n$ are the predicted capacity $\tilde{C}_d(M+n)$, $\tilde{Q}_{\mathrm{CV}}(M+n)$, and $\tilde{B}(M+n)$. However, when predicting the RUL, the measured value of output R could not be acquired. Therefore, we can take advantage of the average degradation parameter $\bar{\lambda}_{R,1:M}$, as shown in (19), to describe the predicted capacity distribution. When the predicted capacity reaches the EoL threshold, the RUL can be regarded as $n+1$.The flowchart of the proposed method can be viewed by drawing a block diagram, as shown in Fig. 9.

IV. Experiments and Verification

A. Verification of the SVR-Based Model

In order to acquire the online C_d estimation model, data from 6# are processed beforehand to train the SVR. The experimental data of 5#, 7#, and 18# are applied to verify the performance of the trained SVR-based model. The experimental results of 5#, 6#, 7#, and 18# are plotted in Fig. 10. To further verify the effectiveness of the SVR-based model, a comparison with the ANN counterpart is conducted. The comparison results are shown in Fig. 10 and Table III. Apparently, the SVR-based model ensures much better performance with considerably less estimation error compared with the ANN-based model, especially about 7# and 18#. The root mean square errors (RMSEs) of the four cells, which can be calculated by the following equation, are 0.0146, 0.0248, 0.0147, and 0.0229 Ah with the SVR-based model, 0.0391, 0.02200 0.0637, and 0.0642 Ah with the ANN-based

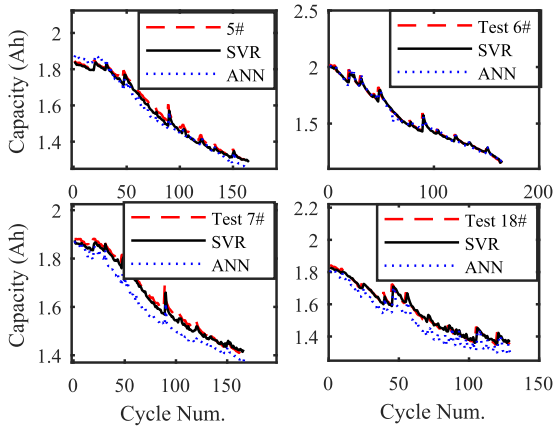

Fig. 10. Verification results of the SVR-based and ANN-based model: the measured and predicted capacity of the four cells.

TABLE III
Numerical Results of SVR-Based Model Verification

Cell num.	5#	6#	7#	18#
SVR RMSE (mAh)	14.6	24.8	14.7	22.9
SVR MaxAE (Ah)	0.12	0.16	0.12	0.14
ANN RMSE (mAh)	39.1	22.0	63.7	64.2
ANN MaxAE (Ah)	0.13	0.15	0.11	0.18

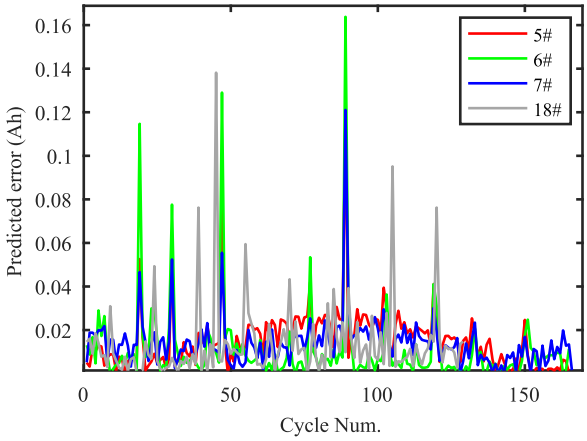

Fig. 11. Absolute estimation errors of four cells.

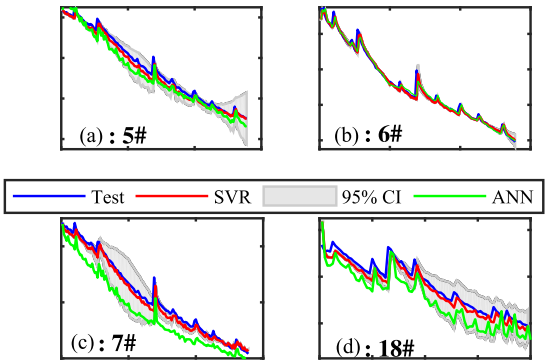

Fig. 12. SOH estimation results: the measured and estimated capacity of (a) 5#, (b) 6#, (c) 7#, and (d) 18#.

model, respectively,

$$\text{RMSE} = \sqrt{\sum_{k=1}^{m}(\widehat{C}_d(k) - C_d(k))^2/m} \tag{20}$$

where m is the total cycle number. Particularly, the absolute estimation errors (AEs) of these cells using the SVR-based model are shown in Fig. 11. According to Figs. 10 and 11, it can be seen that the SVR-based capacity degradation model and actual capacity overlap a lot. The above-mentioned results show that the SVR-based model has been well-trained and can achieve a good capacity estimation accuracy.

B. Verification of SOH Estimation

For the validation of the proposed SOH estimation method, the four cells' aging test data are applied for simulating. The SOH is defined as the ratio of current available capacity to nominal capacity. The SOH estimation results of 5#, 6# 7#, and 18# batteries are shown in Fig. 12(a)–(d), respectively, where the 95% confidence interval (95% CI) is also given. The resistance R estimation results of the four cells are presented by Fig. 13(a)–(d). The numerical results of the PF estimator are listed in Table IV. The RMSEs of the PF-based estimator are 5.1, 8.7, 6.6, and 5.7 mΩ for 5#, 6# 7#, and 18# cells, respectively. To further verify the effectiveness of the SVR-based model, a comparison with the ANN counterpart is conducted, the comparison results are shown in Fig. 13 and Table IV. From Fig. 12, the SOH comparison between estimation and measurement clearly shows that the conformance between estimation and measurement is adequate, although they are different from the discharging cutoff voltages. Furthermore, according to Fig. 13, it can be concluded that the proposed PF-based estimation approach has a relatively high accuracy. These results indicate that the proposed online estimation method is effective for tracking the degradation characteristic of a battery. Besides, it can improve the robustness and reliability of the SOH estimator by combining the SVR-based model and PF estimation method.

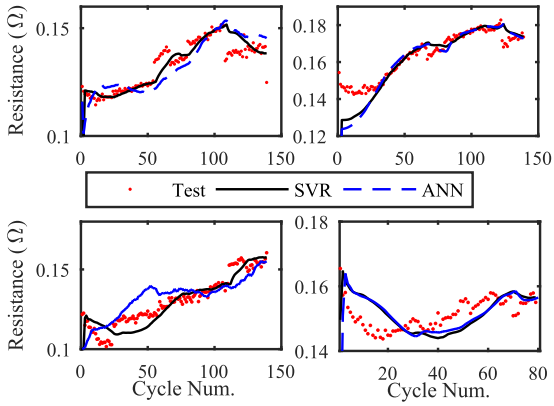

Fig. 13. Resistance (R) estimation results of the four cells using PF.

TABLE IV
NUMERICAL RESULTS OF PF-BASED MODEL VERIFICATION

Cell num.	5#	6#	7#	18#
SVR RMSE (mΩ)	5.1	8.7	6.6	5.7
ANN RMSE (mΩ)	7.2	9.5	9.1	5.9

C. Verification of RUL Prediction

Then, we will discuss the battery RUL prediction results. In this case, the RUL threshold of battery is set to 72% nominal capacity and the RUL will be predicted at cycle number $M = 50$. The predicted battery capacity and RUL results of the four cells are shown in Fig. 14(a)–(d). The numeric results are listed in Table V. The predicted RULs of 5#, 6#, 7#, and 18# batteries are 79, 59, 71, and 29, respectively. The distribution of predicted EOL is assumed as Gaussian, whose variances are 13, 1.1, 25, and 20 for the four cells. These results suggest that the proposed method can predict the RUL in a high estimation accuracy. The accurately predicted RUL values provide valuable pieces of information necessary for the maintenance decision for the degraded LIBs.

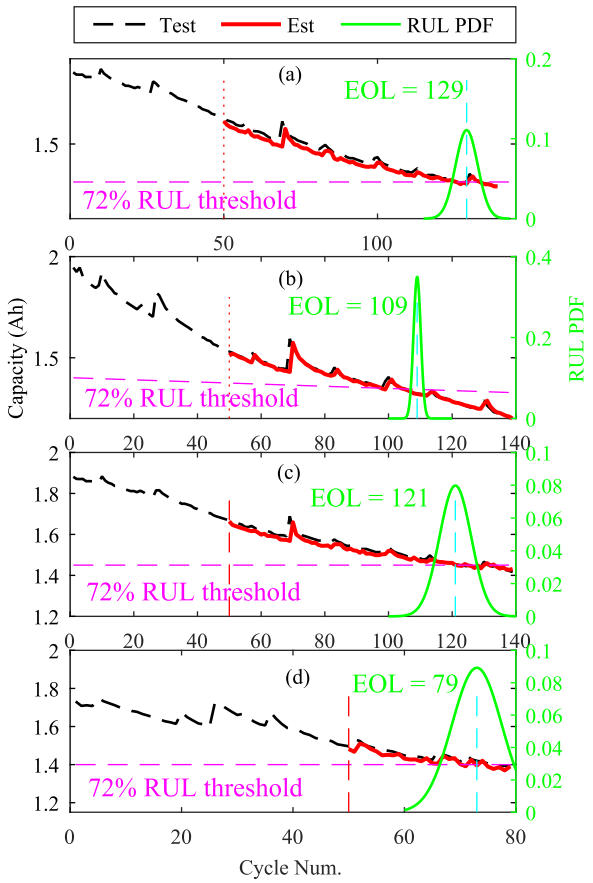

Fig. 14. RUL prediction results of (a) 5#, (b) 6#, (c) 7#, and (d) 18# at $M = 50$.

TABLE V
NUMERIC RESULTS OF RUL PREDICTION

Cell num.	Predicted RUL		Measured RUL
Mean	Variance		
5#	79	13	75
6#	59	1.1	59
7#	71	25	72
18#	29	20	25

V. CONCLUSION

This work focused on SOH diagnosis and RUL prediction of LIBs using support vector regression and particle filter. The battery health parameters including impedance aging parameters and capacity aging parameters were used to estimate battery SOH. First, an SVR-based capacity degradation model was established to describe the dynamic characteristics of battery capacity aging. In this proposed battery degradation model, the representative features during the CC and CV charging protocol were taken as the input variables. When the charging scheme did not always follow the CC and CV protocol, fitting parameters were employed to simulate the capacity degradation characteristics. However, the SVR-based capacity degradation model may introduce prediction errors. To overcome these issues, an impedance aging based degradation parameter model was then established to improve the robustness of the SOH estimator. It can be found from experimental data that the capacity degradation showed a linear relationship with impedance aging. Therefore, impedance degradation parameters can be used to simulate the capacity degradation. A PF was then employed to estimate the degradation parameters. The results showed that the proposed SVR-based model can accurately simulate battery degradation. The proposed battery SOH diagnose method can provide accurate estimation results based on real measured battery parameters. The proposed RUL prediction framework can also ensure accurate RUL prediction results. In the next step, considering the temperature effects on battery aging, it is necessary to analyze battery degradation data at different temperature and dynamic temperature conditions. A more accurate battery degradation model that includes temperature effect could be established by extracting temperature features from collected data.

REFERENCES

[1] G. Dong, X. Zhang, C. Zhang, and Z. Chen, "A method for state of energy estimation of lithium-ion batteries based on neural network model," *Energy*, vol. 90, no. 1, pp. 879–888, Oct. 2015. Doi: 10.1016/j.energy.2015.07.120.

[2] Y. Xiao, "Model-based virtual thermal sensors for lithium-ion battery in EV applications," *IEEE Trans. Ind. Electron.*, vol. 62, no. 5, pp. 3112–3122, May 2015. Doi: 10.1109/TIE.2014.2386793.

[3] J. Wu, Y. Wang, X. Zhang, and Z. Chen, "A novel state of health estimation method of Li-ion battery using group method of data handling," *J. Power Sources*, vol. 327, pp. 457–464, Sep. 2016. Doi: 10.1016/j.jpowsour.2016.07.065.

[4] J. Wu, C. Zhang, and Z. Chen, "An online method for lithium-ion battery remaining useful life estimation using importance sampling and neural networks," *Appl. Energy*, vol. 173, pp. 134–140, Jul. 2016. Doi: 10.1016/j.apenergy.2016.04.057.

[5] S. Tang, C. Yu, X. Wang, X. Guo, and X. Si, "Remaining useful life prediction of lithium-ion batteries based on the Wiener process with measurement error," *Energies*, vol. 7, no. 2, pp. 520–547, Jan. 2014. Doi: 10.3390/en7020520.

[6] H. Chaoui, N. Golbon, I. Hmouz, R. Souissi, and S. Tahar, "Lyapunov-based adaptive state of charge and state of health estimation for lithium-ion batteries," *IEEE Trans. Ind. Electron.*, vol. 62, no. 3, pp. 1610–1618, Mar. 2015. Doi: 10.1109/TIE.2014.2341576.

[7] A. E. Mejdoubi, A. Oukaour, H. Chaoui, H. Gualous, J. Sabor, and Y. Slamani, "State-of-charge and state-of-health lithium-ion batteries' diagnosis according to surface temperature variation," *IEEE Trans. Ind. Electron.*, vol. 63, no. 4, pp. 2391–2402, Apr. 2016. Doi: 10.1109/TIE.2015.2509916.

[8] X. Hu, J. Jiang, D. Cao, and B. Egardt, "Battery health prognosis for electric vehicles using sample entropy and sparse Bayesian predictive modeling," *IEEE Trans. Ind. Electron.*, vol. 63, no. 4, pp. 2645–2656, Apr. 2016. Doi: 10.1109/TIE.2015.2461523.

[9] L. Lu, X. Han, J. Li, J. Hua, and M. Ouyang, "A review on the key issues for lithium-ion battery management in electric vehicles," *J. Power Sources*, vol. 226, pp. 272–288, Mar. 2013. Doi: 10.1016/j.jpowsour.2012.10.060.

[10] G. Dong, J. Wei, and Z. Chen, "Kalman filter for onboard state of charge estimation and peak power capability analysis of lithium-ion batteries," *J. Power Sources*, vol. 328, pp. 615–626, Oct. 2016. Doi: 10.1016/j.jpowsour.2016.08.065.

[11] G. L. Plett, "Extended kalman filtering for battery management systems of LIPB-based HEV battery packs: Part 3. State and parameter estimation," *J. Power Sources*, vol. 134, no. 2, pp. 277–292, Aug. 2004. Doi: 10.1016/j.jpowsour.2004.02.033.

[12] Y. Zou, X. Hu, H. Ma, and S. E. Li, "Combined state of charge and state of health estimation over lithium-ion battery cell cycle lifespan for electric vehicles," *J. Power Sources*, vol. 273, no. 1, pp. 793–803, Jan. 2015. Doi: 10.1016/j.jpowsour.2014.09.146.

[13] D. Andre, C. Appel, T. Soczka-Guth, and D. Sauer, "Advanced mathematical methods of SOC and SOH estimation for lithium-ion batteries," *J. Power Sources*, vol. 224, pp. 20–27, Feb. 2013. Doi: 10.1016/j.jpowsour.2012.10.001.

[14] S. Schwunk, N. Armbruster, S. Straub, J. Kehl, and M. Vetter, "Particle filter for state of charge and state of health estimation for lithium-iron phosphate batteries," *J. Power Sources*, vol. 239, no. 1, pp. 705–710, Oct. 2013. Doi: 10.1016/j.jpowsour.2012.10.058.
[15] I. S. Kim, "A technique for estimating the state of health of lithium batteries through a dual-sliding-mode observer," *IEEE Trans. Power Electron.*, vol. 25, no. 4, pp. 1013–1022, Apr. 2010. Doi: 10.1109/TPEL.2009.2034966.
[16] J. Wang *et al.*, "Cycle-life model for graphite-LiFePO4 cells," *J. Power Sources*, vol. 196, no. 8, pp. 3942–3948, Apr. 2011. Doi: 10.1016/j.jpowsour.2010.11.134.
[17] S. Saxena, C. Hendricks, and M. Pecht, "Cycle life testing and modeling of graphite/LiCoO2 cells under different state of charge ranges," *J. Power Sources*, vol. 327, pp. 394–400, Sep. 2016. Doi: 10.1016/j.jpowsour.2016.07.057.
[18] T. Matsushima, "Deterioration estimation of lithium-ion cells in direct current power supply systems and characteristics of 400-Ah lithium-ion cells," *J. Power Sources*, vol. 189, no. 1, pp. 847–854, Apr. 2009. Doi: 10.1016/j.jpowsour.2008.08.023.
[19] E. M. Krieger, J. Cannarella, and C. B. Arnold, "A comparison of lead-acid and lithium-based battery behavior and capacity fade in off-grid renewable charging applications," *Energy*, vol. 60, pp. 492–500, Oct. 2013. Doi: 10.1016/j.energy.2013.08.029.
[20] L. Wang, C. Pan, L. Liu, Y. Cheng, and X. Zhao, "On-board state of health estimation of LiFePO4 battery pack through differential voltage analysis," *Appl. Energy*, vol. 168, pp. 465–472, Apr. 2016. Doi: 10.1016/j.apenergy.2016.01.125.
[21] M. A. Patil *et al.*, "A novel multistage support vector machine based approach for Li ion battery remaining useful life estimation," *Appl. Energy*, vol. 159, pp. 285–297, Dec. 2015. Doi: 10.1016/j.apenergy.2015.08.119.
[22] A. J. Salkind, C. Fennie, P. Singh, T. Atwater, and D. E. Reisner, "Determination of state-of-charge and state-of-health of batteries by fuzzy logic methodology," *J. Power Sources*, vol. 80, pp. 293–300, Jul. 1999. Doi: 10.1016/S0378-7753(99)00079-8.
[23] H. Dong, X. Jin, Y. Lou, and C. Wang, "Lithium-ion battery state of health monitoring and remaining useful life prediction based on support vector regression-particle filter," *J. Power Sources*, vol. 271, pp. 114–123, Dec. 2014. Doi: 10.1016/j.jpowsour.2014.07.176.
[24] Y. Jiang, Y. Wang, Y. Wu, and Q. Sun, "Fault prognostic of electronics based on optimal multi-order particle filter," *Microelectron. Reliab.*, vol. 62, pp. 167–177, Jul. 2016. Doi: 10.1016/j.microrel.2016.03.030.
[25] M. Charkhgard and M. Farrokhi, "State-of-charge estimation for lithium-ion batteries using neural networks and EKF," *IEEE Trans. Ind. Electron.*, vol. 57, no. 12, pp. 4178–4187, Dec. 2010. Doi: 10.1109/TIE.2010.2043035.
[26] T. Asefa, M. Kemblowski, U. Lall, and G. Urroz, "Support vector machines for nonlinear state space reconstruction: Application to the Great Salt Lake time series," *Water Resour. Res.*, vol. 41, no. 12, pp. 1–10, Dec. 2005. Doi: 10.1029/2004WR003785.
[27] T. Qin, S. Zeng, and J. Guo, "Robust prognostics for state of health estimation of lithium-ion batteries based on an improved PSO SVR model," *Microelectron. Reliab.*, vol. 55, no. 9, pp. 1280–1284, Aug. 2015. Doi: 10.1016/j.microrel.2015.06.133.
[28] F. Li and J. Xu, "A new prognostics method for state of health estimation of lithium-ion batteries based on a mixture of Gaussian process models and particle filter," *Microelectron. Reliab.*, vol. 55, no. 7, pp. 1035–1045, Jun. 2015. Doi: 10.1016/j.microrel.2015.02.025.
[29] B. Saha, S. Poll, K. Goebel, and J. Christophersen, "An integrated approach to battery health monitoring using Bayesian regression and state estimation," in *Proc. IEEE Autotestcon*, 2007, pp. 646–653. Doi: 10.1109/AUTEST.2007.4374280.
[30] K. Goebel, B. Saha, A. Saxena, J. R. Celaya, and J. P. Christophersen, "Prognostics in battery health management," *IEEE Instrum. Meas. Mag.*, vol. 11, no. 4, pp. 33–40, Aug. 2008. Doi: 10.1109/MIM.2008.4579269.
[31] A. Eddahech, O. Briat, and J. M. Vinassa, "Determination of lithium-ion battery state-of-health based on constant-voltage charge phase," *J. Power Sources*, vol. 258, pp. 218–227, Jul. 2014. Doi: 10.1016/j.jpowsour.2014.02.020.

Jingwen Wei (S'17) was born in Hunan, China, in May 1990. She received the B.E. degree in measurement and control technology and instruments from Hefei University of Technology, Hefei, China, in 2013. She is currently working toward the Ph.D. degree in control science and engineering at the University of Science and Technology of China, Hefei, China.

Her research interests include state estimation, balancing and health management, fault diagnosis of lithium-ion batteries in electrical vehicles, and energy storage.

Guangzhong Dong (S'17–M'17) received the B.E. degree in automation in 2013 from the University of Science and Technology of China, Hefei, China, where he is currently working toward the Ph.D. degree in control science and engineering.

His current research interests include dynamic system modeling and control, such as modeling, estimation, health prognosis of energy storage system, optimal energy dispatch, and coordinated control of microgrids.

Zonghai Chen (M'17) received the Bachelor's degree from the Department of Management and Systems Science, University of Science and Technology of China (USTC), Hefei, China, in 1988.

He has been a Professor with the Department of Automation, USTC, since 1998. His main research interests include modeling and control of complex systems, control system engineering and intelligent information processing, energy management technologies for electric vehicles, and smart microgrids.

Prof. Chen is a recipient of special allowances from the State Council of PR China and is a Member of the Robotics Technical Committee of the International Federation of Automation Control.